Nuclear Instruments and Methods in Physics Research B 267 (2009) 1222–1225

Contents lists available at ScienceDirect

Nuclear Instruments and Methods in Physics Research B

journal homepage: www.elsevier.com/locate/nimb

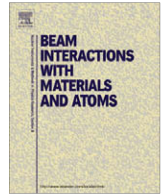

Mapping of ion beam induced current changes in FinFETs

C.D. Weis [a,b], A. Schuh [a,b], A. Batra [a], A. Persaud [a], I.W. Rangelow [b], J. Bokor [c,d], C.C. Lo [c], S. Cabrini [d], D. Olynick [d], S. Duhey [d], T. Schenkel [a,*]

[a] Lawrence Berkeley National Laboratory, 1 Cyclotron Road, Berkeley, CA 94720, USA
[b] Technical University Ilmenau, D-98684 Ilmenau, Germany
[c] Department of Electrical Engineering and Computer Science, University of California, Berkeley, CA 94720, USA
[d] The Molecular Foundry, Lawrence Berkeley National Laboratory, Berkeley, CA 94720, USA

ARTICLE INFO

Article history:
Available online 25 January 2009

PACS:
03.67.−a
61.72.Uf
85.30.Tv
85.40.Ry

Keywords:
Ion beam induced charge (IBIC)
IBIC mapping

ABSTRACT

We report on progress in ion placement into silicon devices with scanning probe alignment. The device is imaged with a scanning force microscope (SFM) and an aligned argon beam (20 keV, 36 keV) is scanned over the transistor surface. Holes in the lever of the SFM tip collimate the argon beam to sizes of 1.6 μm and 100 nm in diameter. Ion impacts upset the channel current due to formation of positive charges in the oxide areas. The induced changes in the source–drain current are recorded in dependence of the ion beam position with respect to the FinFET. Maps of local areas responding to the ion beam are obtained.

© 2009 Elsevier B.V. All rights reserved.

1. Introduction

Kane's proposal of a quantum computer based on donor spin qubits in silicon [1] requires the precise positioning of single dopant atoms in devices integrated with control gates and readout structures. Further, controlled doping of conduction channels in conventional CMOS technology is of interest because device structures are scaled down continuously. Homogeneous doping profiles can no longer be assumed and dopant fluctuations cause fluctuations in device performance [2–5]. We recently demonstrated a spin to charge conversion mechanism with potential for scaling to single spin readout using field effect transistors (FET) [6]. In addition, we demonstrated a technique for single ion doping of these planar FETs by monitoring changes in the source–drain currents at room temperature [7]. The transistor, which was operated in accumulation mode, was exposed to an ion beam and the position of impinging ions into the channel of the FET was defined by a hole in the gate electrode for the detection of single ions. Only ions impinging within this region reached the 2DEG channel and could be detected. Our goal is to place single ions at precise positions by using an SFM with an integrated ion beam (Fig. 1) [8,9]. This allows us to image our devices with no ions hitting the surface, then align the ion beam to desired implantation regions and then implant ions deliberately into selected locations. The ion beam is collimated by holes in a pre-collimator and the cantilever of the SFM tip. The next steps towards ion positioning are scanning this ion beam over the active area of transistors (area that shows response to the impinging ions) and mapping those regions. This approach is common in ion beam induced charge (IBIC) mapping. IBIC can be used as a tool to investigate the uniformity of charge transport in bulk semiconductors; and the influence of extended features such as grain boundaries, precipitates and twins on charge transport [10–12]. Here, we describe our first aligned ion implantation into a device structure that acts as a local detector using our SFM tip. This is a step towards precise positioning of implanted ions and the formation of arbitrary dopant array structures.

2. Experimental setup

FinFETs were fabricated in 250 nm thick SOI (obtained by overgrowth of 50 nm natural silicon on buried oxide with a 200 nm ^{28}Si epi layer). A 100 nm thick low temperature oxide was deposited to serve as the hard mask for the silicon etch. Source/drain pads and channel (fin) regions were defined by electron beam lithography. Channel widths ranged from 30–250 nm (100 nm for shown data). After the silicon etch, a 10 nm thick gate oxide was grown on the sidewalls (∼70 nm on top of fin). In situ phosphorus-doped polycrystalline silicon was deposited as gate electrodes with a thickness of 140 nm. Gates of 280 nm length were patterned by

* Corresponding author. Tel.: +1 510 486 6674; fax: +1 510 486 5105.
E-mail address: T_Schenkel@LBL.gov (T. Schenkel).

0168-583X/$ - see front matter © 2009 Elsevier B.V. All rights reserved.
doi:10.1016/j.nimb.2009.01.019

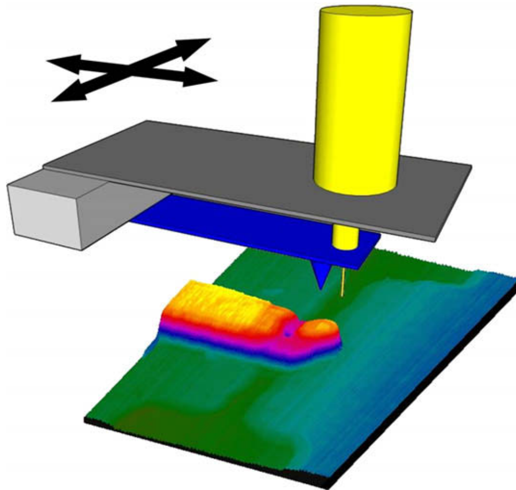

Fig. 1. Schematic of the IBIC mapping procedure.

e-beam lithography and poly silicon dry etching. Self-aligned arsenic implants (25 keV, $2 \times 10^{15}/cm^2$) were used to form source/drain regions. Low-temperature chemical-vapor deposited silicon dioxide (LTO) was used as an interlayer dielectric (capping layer for the fin region) with a thickness of 300 nm. Contact regions were etched and tungsten was used for metal contacts. Devices were annealed in forming gas (N_2/H_2 – 90%/10%) at 400 °C for 20 min to passivate defects at the Si/SiO_2 interface and to improve the metal-semiconductor contact quality. Fig. 2(a) shows the FinFET before LTO film deposition and Fig. 2(b) shows an in situ SFM image after LTO deposition. A dual beam focused ion beam (FIB) system was used to open a hole above the fin of the transistor. First, parts of the LTO layer were removed with a 30 keV Ga^+ ion beam. Then focused electron beam (5 keV) induced etching with

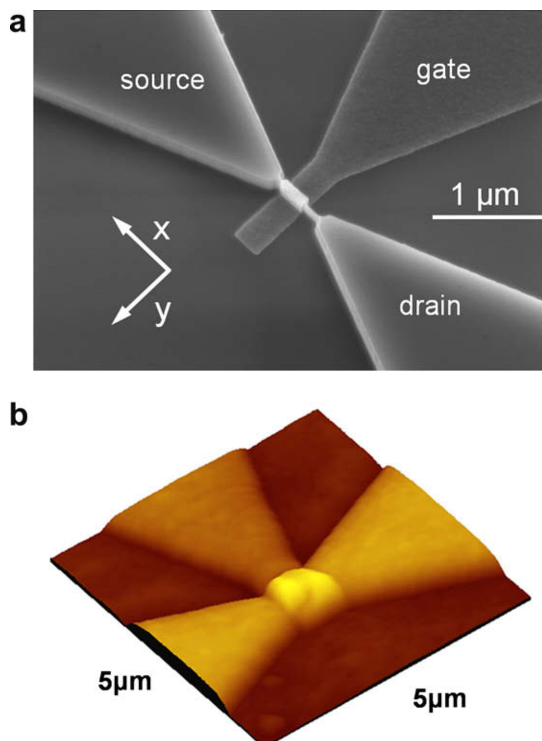

Fig. 2. SEM image of a FinFet before LTO deposition (top). In situ SFM image after LTO deposition (bottom).

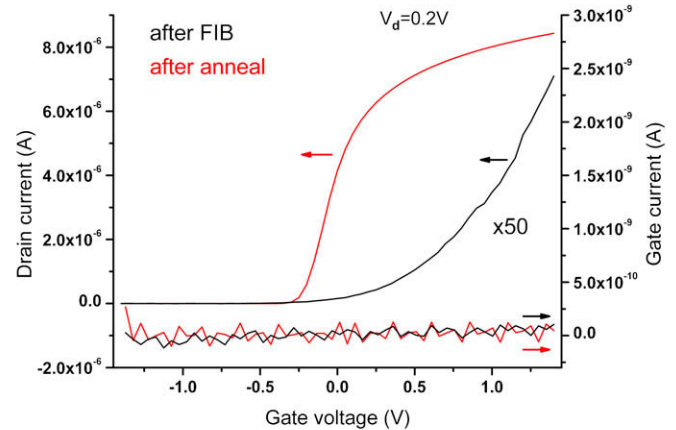

Fig. 3. Room temperature I–V-curves of a FinFET after FIB processing (×50) and after annealing in forming gas.

XeF_2 etch gas was used to drill further into the remaining LTO parts and into the poly silicon gate electrode. The electron beam was turned off for the last part of the etch since XeF_2 alone does etch silicon but not silicon oxide [13,14]. This should lead to an undamaged and exposed gate oxide layer on top of the fin. To what extend the side electrodes were left untouched couldn't be resolved from the SEM images. The exact shape of the drilled hole is subject to further analysis. Important is that the FinFETs did not show any gate leakage and channel currents responded to ion impacts. After FIB processing, the devices were annealed in forming gas (N_2/H_2 – 90%/10%) at 400 °C for 20 min. Electrical device performance was recovered after the anneals (see Fig. 3) and was similar to pre-FIB values. Note that the data after FIB processing is multiplied by a factor of 50 and that the pristine IV-curve is not displayed. Gate leakage currents were below 200 pA. FinFETs were then mounted in our ion implantation setup with aligned SFM. Argon ions were produced in an electron cyclotron resonance (ECR) source [15]. Ar^{3+} (36 keV) and Ar^{2+} (20 keV) ions were extracted and selected with a 90° analyzing magnet and focused onto the sample. Pulsing of the ion beam was achieved by applying a voltage onto a deflector plate parallel to the ion beam trajectory. The devices were operated at a gate bias V_g of 1.0 V, a drain bias V_d of 0.8 V and with the source grounded, resulting in drain currents of approximately 10 µA. The drain current signal was recorded after amplification in a current amplifier (Stanford Research 570). The mounted device was scanned with the SFM and the tip was moved over the FIB drilled area of the FinFET. An offset in x- and y-position was applied so that one of the drilled holes in the SFM cantilever aligned with the FIB drilled hole of the FinFET (x-direction is along the source–drain electrodes and the y-direction is along the gate electrode, see Fig. 2(a)). The distances and directions were obtained from scanning microscope images (SEM), which showed the SFM cantilever and the holes next to the imaging tip. The tip was then moved along each spot of a square point grid. At each spot, the drain current was measured over time and the argon ion beam was turned on for 5 s after a dwell time in which no ions hit the sample. SFM tip position and drain currents were recorded and ion beam exposures were controlled with a Labview program. The total change in the drain current within each interval was plotted versus x- and y-position of the imaging tip to generate the IBIC maps.

3. Results

The data of three consecutive exposure spots is displayed in Fig. 4. Argon ions (36 keV, collimated with the 1.6 µm hole) hit

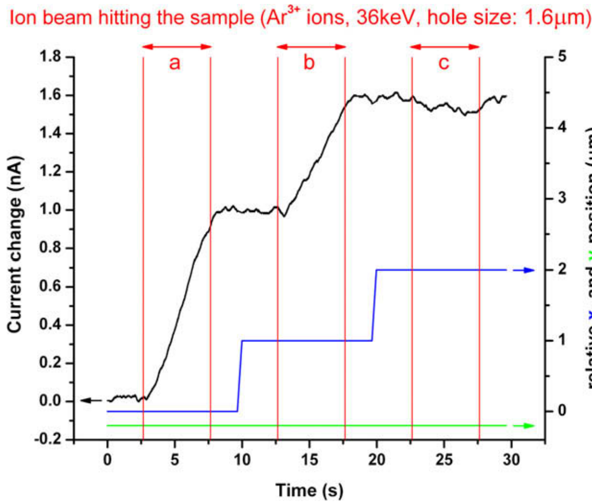

Fig. 4. Example of absolute change of the source–drain current during IBIC map acquisition depending on the *x*- (blue) and *y*-positions (green) of the AFM tip. (For interpretation of the references in colour in this figure legend, the reader is referred to the web version of this article.)

the FinFET during intervals, which are indicated with arrows. The *y*-position is kept constant and the *x*-position is changed by 1 μm between spots. Intervals (a) and (b) show an increase in drain current. No such increase, just the fluctuation of the channel current, can be seen in interval (c). In cases (a) and (b), the tip was in a position in which ions hit areas that resulted in an increase in drain current. As previously demonstrated, ion hits can form positively charged defects in oxides which alter transistor currents [16]. Those positive oxide charges increase the effective gate voltage. The three data sets were obtained when the beam was initially aligned to the gated source–drain region and moved away from that active region. The full set of data for this scan is shown in Fig. 5. Data from 21×21 spots were recorded in a $20 \times 20\ \mu m^2$ area. The exposure time was 5 s for each spot. On average, $\sim$600 ions/s/μm^2 hit the sample (calculated from current reading of the sample and area of the last aperture in front of the sample) and the peaks that correspond to changes in the source–drain current are clearly visible. The beam spot is larger than the distance

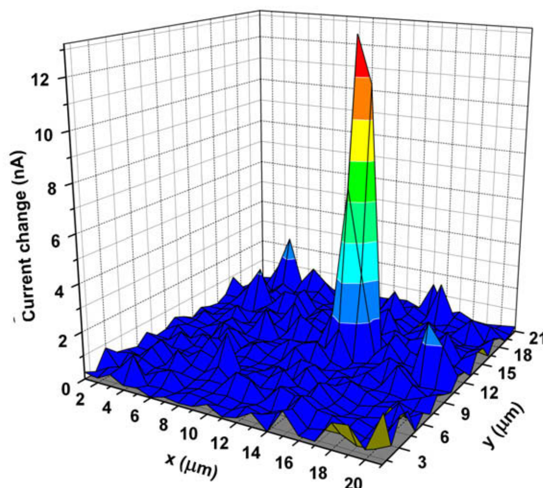

Fig. 5. IBIC map obtained with an argon beam collimated by a 1.6 μm hole in the SFM lever.

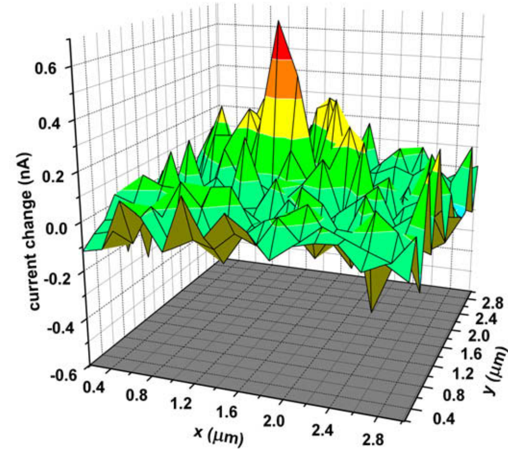

Fig. 6. IBIC response recorded with an argon beam collimated by a 100 nm hole in the SFM lever.

between consecutive spot locations. Therefore, nearest neighbor spots contain responses from the same area. The beam diameter is fairly large compared to the dimensions of the source–drain channel. In order to obtain more accurate maps of the channel region, we collimated the beam with a different hole in the SFM lever which was $\sim$100 nm in diameter. Fig. 6 shows one of the IBIC maps obtained with argon ions (20 keV). The exposure time was set to 30 s per spot and the beam fluence was $\sim$1500 ions/s/μm^2. The distance between spots was 200 nm and 16×16 spots were exposed within a $3 \times 3\ \mu m^2$ area. The signal ratio of active area to surrounding area is smaller than in Fig. 5. The fluence of the 20 keV ions was 2.5 times higher than the fluence of the 36 keV ions. Accounting the difference in fluence and the total deposited energy in the silicon oxide for the different ion energies, the total deposited energy is similar (SRIM simulation [17]). With an average creation energy for electron hole pairs of 18 eV in silicon oxide [18] the expected response to the ion beam would be similar. The smaller response could be explained by the difference in the size of the holes in the cantilever. In the case of the smaller hole, only parts of the total active area were exposed, whereas beam spots collimated with the larger hole exposed most of the entire active area at once. In both circumstances, four beam positions resulted in a channel current response. The large hole beam-spots were overlapping whereas the small hole beam-spots were separated. The active area can be estimated to be around 400–600 nm in side length. This is larger than we would have expected from the fin dimension of $100 \times 280\ nm^2$. No single ion hits were observed and relatively high ion fluences were needed to observe changes in the channel current. One possible explanation is that the LTO and gate material on top of the fin were not removed completely. Impinging ions may have created positively charged defects in the LTO layer instead of the gate oxide as previously observed [7].

4. Discussion and outlook

This paper shows aligned ion implantation onto a surface feature that acts as a local detector. Thus far, patterns were generated on samples without in situ ion detection [8,9,19] and impinging ions on the surface were detected while the whole sample was exposed [7]. In the present study, the ion beam was pre-collimated, the desired implantation region was scanned with the SFM, the tip was aligned to the source–drain region and the ion beam was scanned over a small area to map the responsive areas of our de-

vices. This is an important step towards our goal of precision ion implantation and will act as an in situ calibration method for our tips in the future. The resolution of the maps will be increased by collimating the beam further down. Calibration will improve the positioning of the tip and alignment of the ion beam to selected implant locations. We are in the process of improving the LTO and gate electrode removal process in order to combine the detection of single ions with the IBIC mapping. This will enable us to study the effects on device performance, e.g. change in the threshold voltage, caused by the number and position of donor atoms. Since the devices survive activation anneals, consecutive implantations are possible and will be monitored and correlated to changes in device behavior.

Acknowledgments

We thank the staff of the Microlab at UC Berkeley and the staff of the Molecular Foundry and the National Center for Electron Microscopy at LBNL for their support. This work was supported by NSA under Contract Number MOD 713106A, the National Science Foundation through NIRT Grant No. CCF-0404208 and by the Director, Office of Science, of the Department of Energy under Contract No. DE-AC02-05CH11231.

References

[1] B.E. Kane, Nature (London) 393 (1998) 133.
[2] R.W. Keyes, Appl. Phys. 8 (1975) 251.
[3] T. Mizuno, J. Okamura, A. Toriumi, IEEE Trans. Electr. Dev. 41 (1994) 2216.
[4] H.P. Wong, Y. Taur, D.J. Frank, Micro. Rel. 38 (1998) 1447.
[5] T. Shinada, S. Okamoto, T. Kobayashi, I. Ohdomari, Nature 437 (2005) 1128.
[6] C.C. Lo, J. Bokor, J. He, A.M. Tyryshkin, S.A. Lyon, T. Schenkel, Appl. Phys. Lett. 91 (2007) 242106.
[7] A. Batra, C.D. Weis, J. Reijonen, A. Persaud, S. Cabrini, C.C. Lo, J. Bokor, T. Schenkel, Appl. Phys. Lett. 91 (2007) 193502.
[8] A. Persaud, S.J. Park, J.A. Liddle, J. Bokor, I.W. Rangelow, T. Schenkel, Nano Lett. 5 (2005) 1087.
[9] A. Persaud, J.A. Liddle, T. Schenkel, J. Bokor, Tzv. Ivanov, I.W. Rangelow, J. Vac. Sci. Technol. B 23 (2005) 2798.
[10] P.J. Sellin, A.W. Davies, F. Boroumand, A. Lohstroh, M.E. Ozsan, J. Parkin, M. Veale, Semiconductors 41 (2007) 395;
J. Shen, D.K. Aidun, L. Regel, W.R. Wilcox, Mat. Sci. Eng. B 16 (1993) 182.
[11] G. Vizkelethy, B.L. Doyle, D.K. Brice, P.E. Dodd, M.R. Shaneyfelt, J.R. Schwank, Nucl. Instr. and Meth. B 231 (2005) 467.
[12] M.B.H. Breese, D.N. Jamieson, P.J.C. King, Materials Analysis Using a Nuclear Microprobe, John Willy & Sons, New York, 1996 (and references therein).
[13] H.F. Winters, J.W. Coburn, Appl. Phys. Lett. 34 (1979) 70.
[14] S.J. Randolph, J.D. Fowlkes, P.D. Rack, J. Appl. Phys. 98 (2005) 034902.
[15] J. Reijonen, M. Eardley, R. Gough, K. Leung, R. Thomae, Nucl. Instr. and Meth. A 511 (2003) 301.
[16] T.A. Ma, Paul V. Dressendorfer, Ionizing Radiation Effects in MOS Devices & Circuits, Wiley, New York, 1989. p. 1.
[17] The Stoping Range of Ions in Matter, version 2006.02, <www.srim.org>.
[18] G.A. Ausman Jr., F.B. McLean, Appl. Phys. Lett. 26 (1975) 173.
[19] C.D. Weis et al., J. Vac. Sci. Technol. B 26 (6) (2008) 2596.